



Relationships between char reactivity and char structure from a suite of organic model compounds

Zhengyan Bao^{a,b}, Zhimin Lu^{a,b,*}, Jinzheng Chen^{a,b}, Jianfeng Cai^{a,b}, Shengyuan Guo^{a,b}, Shunchun Yao^{a,b}

^a School of Electric Power, South China University of Technology, 510640 Guangzhou, China

^b Guangdong Province Key Laboratory of Efficient and Clean Energy Utilization, 510640 Guangzhou, China

ARTICLE INFO

Keywords:

Organic model compounds
Char reactivity
Carbon structure
TGA
Raman spectroscopy

ABSTRACT

In order to better understand the impact of the carbon structure of char on its combustion reactivity, 14 types of organic model compounds were pyrolyzed under temperatures of 530 °C, 800 °C and 1028 °C at heating rates of 10 °C/min and 65 °C/s, respectively. The carbon structure and the oxidation reactivity of the produced char were determined by respective Raman spectroscopy and thermogravimetric analysis (TGA) methods. The relationships between different reactivity indexes and Raman spectral parameters have been assessed. The results reveal that changes in pyrolysis temperature and heating rate would result in certain evolution of the graphitization degree of char. Good correlations have been discovered between the Raman spectral parameters (A_D/A_{ALL} , A_{GL}/A_{ALL} , $A_{(S+R+SL+VR+VL)}/A_D$, and $A_{(GR+VL+VR)}/A_D$) and the combustion characteristic temperatures (T_i , T_b , T_{50} , and T_{max}). From the correlations above, Raman spectral parameter $A_{(GR+VL+VR)}/A_D$ is found to be the best correlated to the char combustion characteristic temperature T_b with R^2 of around 0.76.

1. Introduction

Combustion is an important thermochemical process for solid fuels. Compared with the devolatilization process, char conversion is known as the rate-limiting step [1]. Hence the reactivity of char is usually regarded as an important factor in solid fuel application. It is significantly impacted not only by the physicochemical properties of feedstock but also by the pyrolysis conditions, both of which greatly affect the char's properties [2–4]. Due to the diversity of biomass types and char production techniques, the properties and reactivity of char may vary substantially. To achieve target product quality in existing industrial facilities, the combustion procedure has to keep changing to meet the reactivity of the current fuel, which will therefore cause costly process modifications [5]. Hence the reactivity of chars derived from different feedstock should be further investigated.

It is well known that the char carbonaceous structure and catalytic mineral species in char affect char reactivity [6]. Several investigations have shown that the inorganic mineral content has the greatest impact on the reactivity of char among all the factors, as it can either catalyze or inhibit the reaction. For example, the ratios of inorganic composition

like K/Si [7], K/(Si + P) [8,9], and $K_2O/(SiO_2 + Al_2O_3 + P_2O_5)$ [10,11] are all proved to be well connected to the char reactivity. The carbon structure of char, however, also shows a significant effect on char reactivity when the influence of inorganic matter is minimized or removed. Asadullah et al. [12] studied the effect of biomass char structure on its reactivity and discovered that the condensation of aromatic ring systems could be reflected in the reactivity of biomass char. According to the research by Wu et al. [13], the carbon structure of acid-treated char controlled its reactivity while removing the inorganic chemicals. Tay et al. [14] investigated chars with similar Na concentrations. They discovered that the decrease in char reactivity was mostly attributed to the changes in the char structure and that a higher concentration of O-containing structures in char was correlated to a higher level of char reactivity.

Biomass feedstock is a complicated natural polymer made mostly of lignocellulosic structural components, extractives, and minerals [15]. Because of the low levels of potentially catalytic inorganic matter, model compounds, such as xylose, cellobiose, and glucose, were chosen as mineral-free feedstock [16–18]. As they can eliminate the interference of the mineral elements on the biomass pyrolysis and combustion

* Corresponding author at: School of Electric Power, Guangdong Province Key Laboratory of Efficient and Clean Energy Utilization, South China University of Technology, No. 381 Wushan Road, Tianhe District, Guangzhou 510640, China.

E-mail address: zhmlu@scut.edu.cn (Z. Lu).

<https://doi.org/10.1016/j.fuproc.2023.107852>

Received 18 March 2023; Received in revised form 18 May 2023; Accepted 21 May 2023

Available online 30 May 2023

0378-3820/© 2023 Elsevier B.V. All rights reserved.

reactivity, it provides a better understanding of the impact of the char structure properties on the reactivity of char from the thermal conversion of biomass. Lang and Hurt [19] measured the char combustion reactivity of 31 feedstock which included 20 solid fuels and 11 organic model materials that are essentially devoid of the inorganic elements, which are ubiquitous in solid fuels, and identified quantitative relationships between the char reactivity and the properties of feedstock. Their results showed that using the percentage carbon content of the feedstock (C wt%, dry-ash-free, daf) of the source fuels, the reactivity could be estimated to some extent. The findings revealed a correlation between reactivity and C wt% of coals across a wide range of C wt%, but it was a poor predictor of char reactivity of biomasses and their model compounds. Based on the research of char from biomass components, Zhang et al. [20] inferred that the elemental composition of the char samples was closely related to the char reactivity, and a low C content and high H, O, N, and S contents can promote char gasification reactivity. Existing research has shown potential for the study of the relationships between char reactivity and their carbon structures by investigating the combustion behavior and structural properties of char from the pyrolysis of various types of organic model compounds. The research on the structural properties and combustion behavior of char from the organic model compounds also help to make a better understanding of the overall pyrolysis and combustion mechanism of real biomass.

To examine the char structure, a number of characterization tools, including Fourier transform infrared spectroscopy (FT-IR), Raman spectroscopy, X-ray fluorescence spectrometer (XRF) and X-ray diffraction (XRD) etc., have been employed [10,21,22]. Raman spectroscopy is becoming increasingly used for studying the microstructures of char since it is very effective, nondestructive and precise [23]. Raman spectroscopy has been utilized by several researchers to examine the composition and properties of char produced by the thermal conversion of biomass. Xu et al. [24] investigated the char property of the pyrolysis of three typical biomasses using Raman spectroscopy. The changes in Raman band position and bandwidth characteristics reveals that the ordering degree of the char structure increases progressively with increasing pyrolysis temperature and that the carbon structure of different biomass char varies significantly. Guizani et al. [25] used Raman spectroscopy to study the effect of heat treatment conditions on the properties of char. In their research, different TGA reactivity variables, such as dm/dt_{mean} , T_{50} , and R_{index} , were discovered to be closely correlated with O/C, total Raman area (TRA), and I_V/I_D , respectively, revealing close links between char chemical composition, structure, and reactivity. Zhong et al. [26] found that for char derived from solar pyrolysis of biomass pellets, Raman parameters showed different trends of decrease between surface and inner char during the last stage of pyrolysis, indicating that the carbonization process of these two kinds of char followed different paths. Li et al. [27] investigated the biomass-coal reburning behavior and found that Raman parameter $I_{(GR+VL+VR)}/I_D$ of coal char was lower than that of char from the mixture of coal and biomass, and the combustion reactivity of the former was also lower than that of the latter. Unfortunately, their researches didn't make further investigation of the relationships between the Raman parameters and the combustion reactivity, and the number of feedstock in their studies was also limited. Thus, it is worthwhile to investigate the structures of various kinds of biomass model compounds by Raman spectroscopy and establish connections between the char reactivity and the Raman spectral parameters.

In this study, 14 types of organic model compounds, including the three main components of biomass, commercial organic chemical reagents, resins, etc., that differ in C wt% of feedstock, were pyrolyzed under different temperatures and heating rates to acquire chars with different graphitization degree. The char reactivity was obtained by the TGA, and the evolution of the char structure was characterized by the Raman analysis. The current research is aimed at analyzing the char structures using the Raman spectroscopy from the pyrolysis of a large

number of organic model compound samples with varying C wt% and attempts to establish the relationships between the char combustion reactivity and the carbon structure that is represented by the Raman spectral parameters.

2. Materials and methods

2.1. Material

In the present study, 14 different types of model compounds were considered as feedstock. Glucose, D-xylose, amylopectin, starch, sucrose, D-(+)-cellobiose, pectin, L-ascorbic acid 6-palmitate, phenol-formaldehyde resin, and polycarbonate resin were obtained from Macklin; cellulose was obtained from Aladdin; xylan was obtained from Sigma-Aldrich; and two types of lignin were obtained from Macklin and Sigma-Aldrich, respectively. All the samples were dried at 105 °C overnight before the pyrolysis experiment.

2.2. Char preparation

The pyrolysis experiments were conducted in a three-heating-zone tube oven, the description of which can be seen in our previous work [28]. In each experiment, 420(±1) mg of sample was used and spread evenly on the porcelain boat. 20 L of N₂ were purged into the oven at a flow rate fixed to 1 L/min prior to each experiment and maintained an inert atmosphere throughout the pyrolysis process.

The temperature and the heating rate were changed for a parametric study. The pyrolysis was carried out at 530 °C, 800 °C, and 1028 °C, respectively. Two distinct heating rates were chosen for the pyrolysis experiment: 10 °C/min as a slow heating rate and roughly 65 °C/s as a fast heating rate [28]. The holding time at the peak temperature of pyrolysis was set as 20 min.

2.3. Elemental analysis of feedstock and char

The elemental analysis of samples was conducted in a CHN analyzer (SUNDY SDCHN 435). The C, H, and N contents were directly obtained from the test, and the content of O was calculated by subtraction. The elemental analysis results for the feedstock and char are shown in Table S1.

2.4. Characterization of char

The Raman spectrum of the char samples of the model compounds was characterized by a Raman spectrometer (LabRAM Aramis) at 633 nm laser excitation. In this study, the first-order Raman spectra between 800 and 1800 cm⁻¹ were curve-fitted with 10 Gaussian bands according to the method proposed by Li et al. [29]. The assignments and descriptions of each band are listed in Table 1. One sample of curve-fitting for a char from the pyrolysis of cellulose is shown in Fig. 1. The average band area of the ten bands for curve-fitting the spectrum is shown in Table S3.

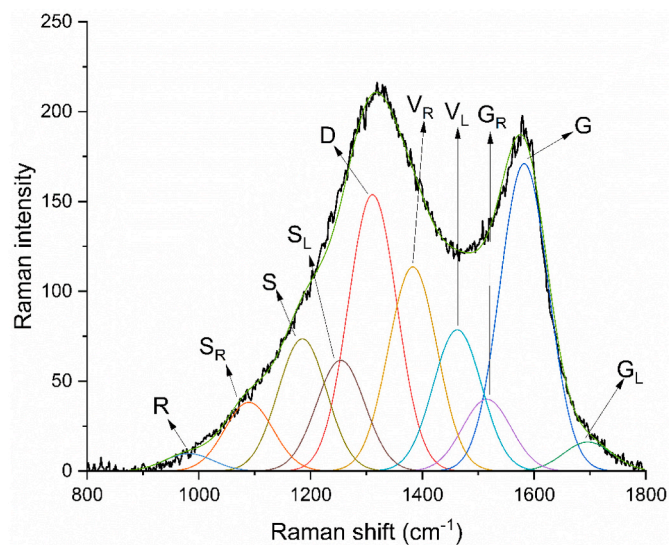
2.5. Thermogravimetric analysis

The char combustion experiments were conducted in a thermogravimetric analyzer (NETZSCH STA 409F1). About 2.5 mg of chars were combusted non-isothermally at a heating rate of 10 °C/min to 800 °C. The combustion atmosphere in the TGA furnace was N₂ and O₂, and the gas flow rate was 95 mL/min and 5 mL/min, respectively. Samples of TG results of char from pyrolysis of cellulose are shown in Fig. 2. Characteristic temperatures were used as the indicators for char reactivity; the char with higher characteristic temperatures is considered with lower reactivity [31,32]. Such characteristic temperatures include the ignition temperature (T_i), the burnout temperature (T_b), the temperature corresponding to 50% conversion (T_{50}), and the temperature at which the

Table 1

A summary of the Raman bands assignment [23,29,30].

Band position, cm^{-1}	Band name	Description
800–960	R	C–C on alkanes and cyclic alkanes; C–H on aromatic rings
1060	S_R	C–H on aromatic rings; benzene ring
1185	S	$C_{\text{aromatic}}-C_{\text{alkyl}}$; aromatic (aliphatic) ethers; C–C on hydro-aromatic rings; hexagonal diamond carbon sp^3 ; C–H on aromatic rings
1230	S_L	Aryl-alkyl ether; para-aromatics
1320	D	D band on highly ordered carbonaceous materials; C–C between aromatic rings and aromatics with no less than 6 rings
1380	V_R	Methyl group; semi-circle breathing of aromatic rings; amorphous carbon structures
1465	V_L	Methylene or methyl; semi-circle breathing of aromatic rings; amorphous carbon structures
1540	G_R	Aromatics with 3–5 rings; amorphous carbon structures
1580	G	Graphite E_{2g}^2 ; aromatic ring quadrant breathing; alkene C=C
1680	G_L	Carbonyl group C=O

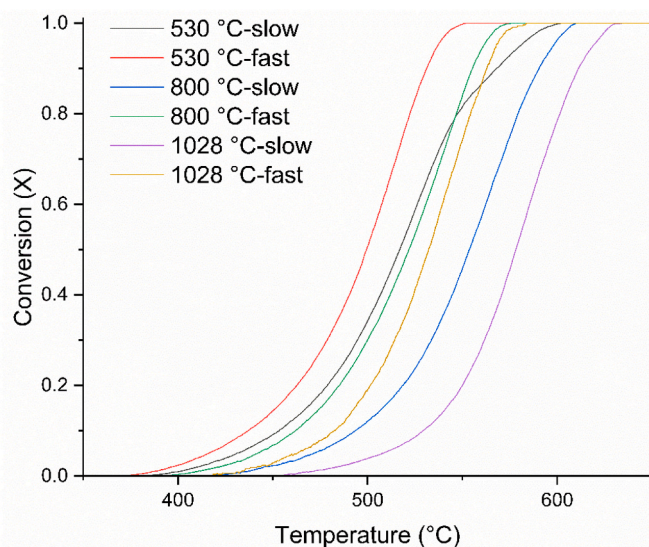
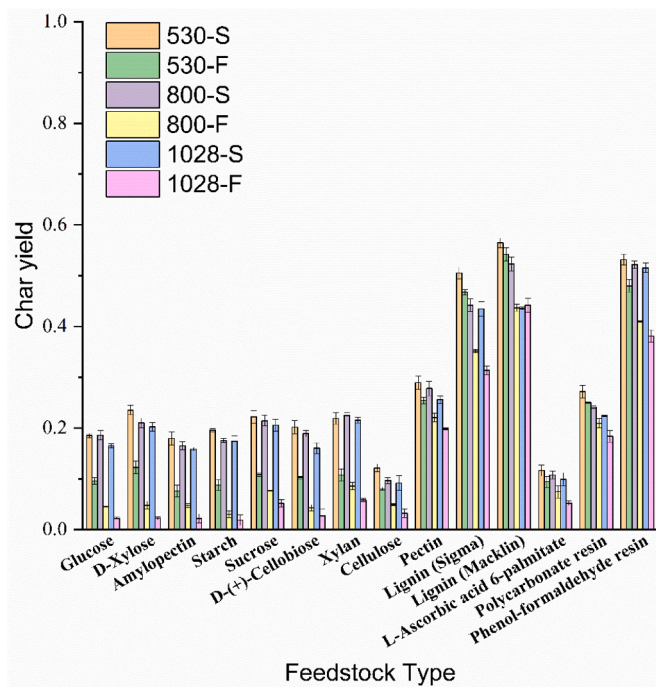
**Fig. 1.** Curve-fitting of a Raman spectrum of the char from slow pyrolysis of cellulose at 800 °C.

maximum rate of mass loss occurred (T_{max}). In this investigation, T_1 and T_b , and T_{max} were derived from Thermogravimetric (TG) and differential Thermogravimetric (DTG) curves, which have been widely employed by researchers [33–35]. An example of the access of the characteristic temperatures is shown in Fig. S1. These four characteristic temperatures were used to reflect the combustion characteristics of the char and depict the reactivity of the char in this study. Detailed information on the four characteristic temperatures of the chars in this study is listed in Table S2.

3. Results and discussion

3.1. Effect of pyrolysis condition on char yield and atomic ratios

Fig. 3 illustrates the effects of the heating rate (slow versus fast heating) and pyrolysis temperature (530, 800, and 1028 °C) on the yields of the chars from the pyrolysis of the model compounds in nitrogen. It shows that the selected model compounds produced less char when the temperature was raised (as seen in Fig. 3). When the pyrolysis temperature increased from 530 °C to 800 °C, the average char yield of

**Fig. 2.** Sample mass as a function of temperature in the oxidation reaction of chars from pyrolysis of cellulose.**Fig. 3.** Char yield of 14 model compounds under pyrolysis at 530 °C, 800 °C, and 1028 °C at heating rates of 10 °C/min (denoted as S, slow) and 65 °C/s (denoted as F, fast).

these model compounds dropped by 1.90% of their initial dried mass. The average char yield of these model compounds was further reduced by 1.68% when the pyrolysis temperature was raised from 800 °C to 1028 °C. The rapid heating causes the char yield to vary more with the temperature compared to the slow heating rate. In particular, the production of the chars increased by 5.26% from 530 °C to 800 °C and by 2.19% from 800 °C to 1028 °C. During the pyrolysis of the model compounds in this study, it was discovered that the heating rate had a greater impact on the char yield than the pyrolysis temperature. The average yield of char produced by the fast pyrolysis at 530 °C, 800 °C, and 1028 °C was 6.94%, 10.30%, and 10.80% lower than the yield of char produced by the slow pyrolysis, respectively. It is known to all that

the volatiles escape from the particle at a much faster rate when the heating rate is high. Hence less time is available for subsequent charring processes, which also enhances the breakdown of the organic constituents [28,36]. The char yield data in Fig. 3 is ordered by the C wt% in the feedstock. There appears to be no discernible effect of feedstock property on char yield, i.e., the higher carbon content in the feedstock does not guarantee a higher char yield.

The Van Krevelen diagram, which lists 84 distinct forms of char from the pyrolysis of different model compounds, is shown in Fig. 4. This study reveals that the amount of oxygen in the char is not very high and that the ratio of oxygen to carbon in atoms decreases linearly with the atomic ratio of hydrogen to carbon decreasing. This is most likely owing to the fact that the pyrolysis temperature in this study exceeded 500 °C, and the char condensation took place more frequently [37]. It can be seen in Fig. 4 that when pyrolyzed at a high temperature, especially higher than 500 °C, the hydrogen in aromatic systems escapes continuously from the char, whereas the extremely little residual oxygen forms cross-linking structures and continues to release slowly as a result [38]. The R^2 (coefficient of determination) value for the correlation between O/C and H/C for the char is roughly 0.79, indicating an approximatively linear relationship between the two ratios. The heating rate of the pyrolysis processes seems to have no effect on the elemental concentration, as Fig. 4 indicates that char from two distinct heating rates has almost the same correlation between O/C and H/C.

3.2. Effect of pyrolysis condition on char structure

In order to further investigate the changes in char structure during pyrolysis, each Raman spectrum was deconvoluted into 10 Raman bands. Fig. 5 shows the ratios between the peak areas of selected Raman bands, including A_D/A_{ALL} , A_{GL}/A_{ALL} , $A_{(S+R+SL+VR+VL)}/A_D$, and $A_{(GR+VL+VR)}/A_D$.

The ratio of the D band to the area of all the bands from 800 to 1800 cm^{-1} (A_D/A_{ALL}) with the increase of pyrolysis temperature is shown in Fig. 5a. This ratio indicates the primary Raman contribution from big

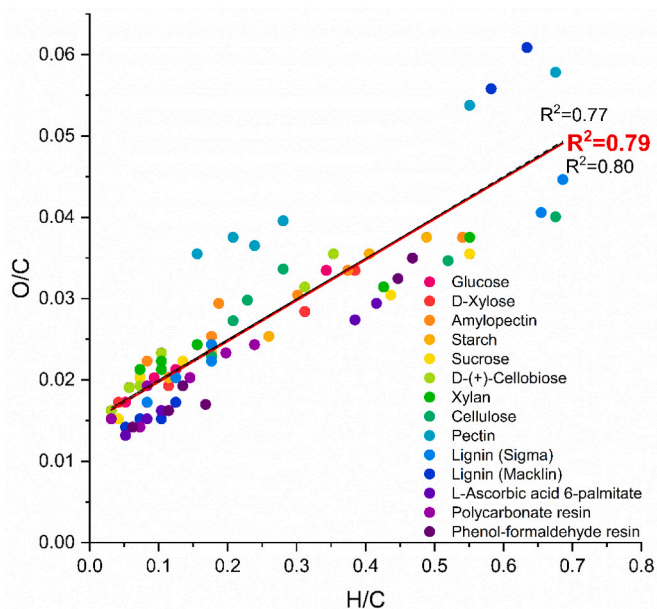


Fig. 4. The Van Krevelen diagram of char samples produced from 14 model compounds under pyrolysis temperatures from 530 °C to 1028 °C at heating rates of 10 °C/min and 65 °C/s. The solid black line represents the linear fitting of char from a fast heating rate, the dash black line represents the linear fitting of char from a slow heating rate, and the red line represents the linear fitting of all char samples. (For interpretation of the references to colour in this figure legend, the reader is referred to the web version of this article.)

aromatic ring systems (no less than six fused rings) [39–41]. The tendency for all the chars with the pyrolysis temperatures from 530 °C to 800 °C is an increase in the relative contribution of the D band structures to the measured Raman spectra, which becomes reasonably steady or drops somewhat from 800 °C to 1028 °C. The proportional increase in the concentrations of the large aromatic ring systems, which have six or more fused benzene rings, is shown by the early rises in the A_D/A_{ALL} ratio, which occur between 530 °C and 800 °C. This occurs as a direct consequence of the dehydrogenation of the hydroaromatics to form larger aromatic systems in the char during the pyrolysis at temperatures in the range specified above [38]. At temperatures greater than 800 °C, further ring condensation may form larger aromatic ring systems (up to six fused benzene rings) that are Raman active in the D band. However, the further condensation of the aromatic rings will lead to the decrease of the ‘defect’ structures, which would cause the tendency to lower the Raman intensity at the D band [29].

Fig. 5b illustrates the change in the ratio of the area of the G_L band to the area of all the bands (A_{GL}/A_{ALL}) that occurs when increasing the pyrolysis temperature. The changes in the concentration of the carbonyl group $\text{C}=\text{O}$ in char are primarily responsible for this shift [26,29,42,43]. It was found that the ratio tended to decrease when the pyrolysis temperature increased from 530 °C to 800 °C and remained steady when the temperature kept increasing from 800 °C. Worth noting there was a significant reduction in the amount of the O-containing groups, such as the carbonyl group, when the temperature of pyrolysis increased. This was notably true for pyrolysis temperatures ranging from 530 °C to 800 °C. Moreover, after that, it turned out to be typically stable when subjected to higher temperatures for the reason that the O-containing groups had been almost completely consumed.

The variations that occur in the proportion of the areas of the S, R, S_L , V_R , and V_L bands to the area of the D band can be seen in Fig. 5c. These bands have some sort of connection to the structures that have partial sp^3 properties, such as the penta-fused (5-membered) ring systems and the O-containing structures, which can be found in the chars produced from the biomass, but disappear in the graphite [29,41]. When the pyrolysis temperature is raised, there is a general tendency for all these chars to experience a reduction in the ratio $A_{(S+R+SL+VR+VL)}/A_D$. It means that these structures are likely to be among the desirable structures that are consumed during the pyrolysis process [26,41,44,45]. The ratio $A_{(S+R+SL+VR+VL)}/A_D$ is seen to decrease from 530 °C to 800 °C for all samples and to decrease less or remain unchanged from 800 °C to 1028 °C. It can be revealed from Fig. 5c that these structures are present at 530 °C and gradually disappear by increasing the pyrolysis temperature. In addition, the char structure will become increasingly organized as the pyrolysis temperature rises [46].

As the pyrolysis temperature increases, Fig. 5d depicts how the ratio of the areas of the G_R , V_L , and V_R bands to the area of the D band shifts. The ratio $A_{(GR+VL+VR)}/A_D$ is interpreted as a relative measurement of the ratios between the smaller (2–5 fused benzene rings) and the larger (more than six rings) aromatic ring systems in char [26,41,47–51]. It is abundantly obvious that the majority of char showed a decrease in $A_{(GR+VL+VR)}/A_D$ when the pyrolysis temperature was raised. It means that the small aromatic ring systems are consumed during pyrolysis. The condensation of the aromatic ring systems leads to a transition of the smaller aromatic ring systems (3–5 fused rings) into larger ones (no less than six fused rings).

Fig. 5 further infers how the features of the char structure are affected by the rate of heating. It’s interesting to note that the A_D/A_{ALL} ratio for the fast heating rate was often lower than that for the slow heating ones. On the other hand, the A_{GL}/A_{ALL} ratio, the $A_{(S+R+SL+VR+VL)}/A_D$ ratio, and the $A_{(GR+VL+VR)}/A_D$ ratio of the fast heating rate were all greater. These findings indicated that pyrolyzed with a slow heating rate resulted in a longer time spent by the char at high temperature compared with the experiments at a fast heating rate, which ultimately led to a greater amount of reaction of condensation [52,53]. In addition, it can be observed from Fig. 5 that most of the

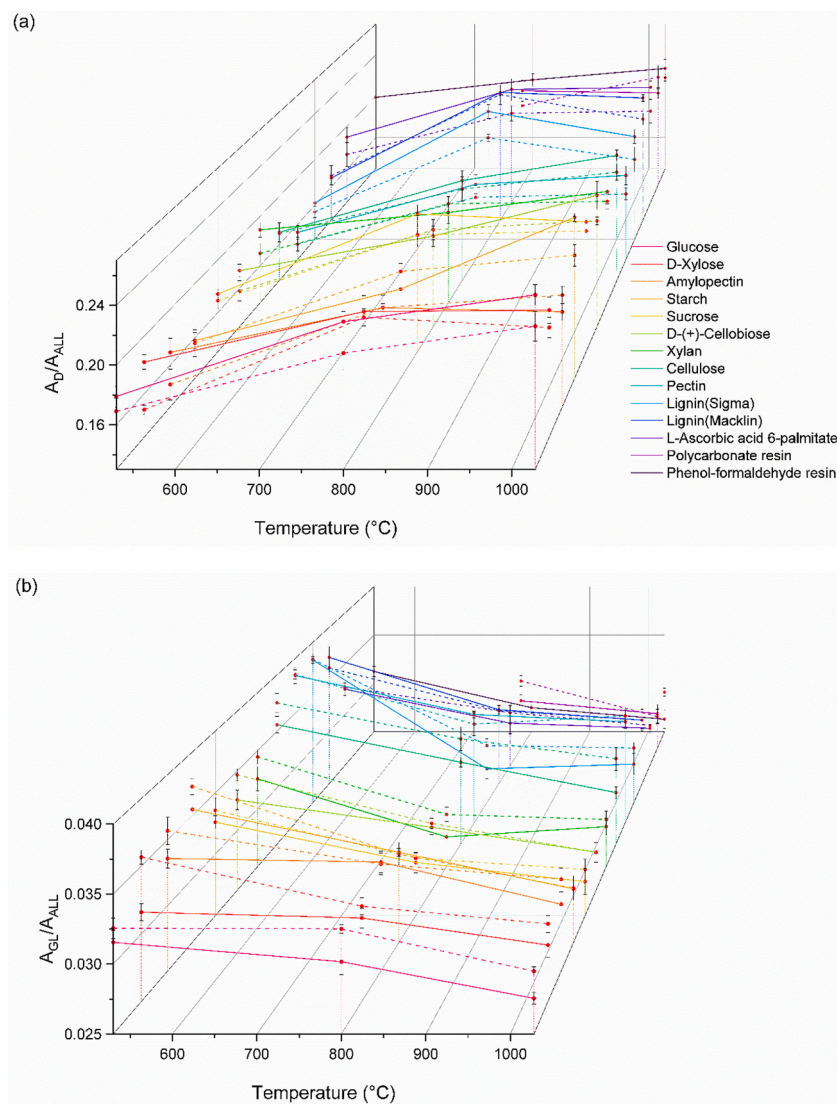


Fig. 5. The change of ratios of Raman band areas (a) A_D/A_{ALL} , (b) A_{GL}/A_{ALL} , (c) $A_{(S+R+SL+VR+VL)}/A_D$, and (d) $A_{(GR+VL+VR)}/A_D$ as a function of pyrolysis temperature. The solid line and dash line represents fast pyrolysis and slow pyrolysis, respectively.

organic model compound-derived chars showed similar trends for the changes in the pyrolysis conditions. It implies that these trends are universal for chars derived from organic model compounds in this study.

3.3. Carbon structure reflected by elemental analysis

It is well known that the elemental contents of C, H, and O are significant indexes of char structural property. As the temperature of the pyrolysis process rises, elemental analysis reveals that an increasing amount of oxygen and hydrogen is lost as a result of deoxygenation and dehydration [54,55]. As a direct consequence of this, both the H/C and O/C ratios become lower. The ratio of hydrogen to carbon is proportional to the amount of the fused aromatic ring structures, and its decrease is a result of the aromatization and carbonization of char [56]. The O/C ratio is used to describe the stability of the char, and a relatively lower O/C ratio implies that a char has a high fraction of stable carbon [36,57]. Hence, the loss of oxygen and hydrogen is indicative of the ordering or condensation of the char structure [2,58]. Thus, comparing the relative changes in the proportions of C, H, and O may be useful to investigate the development of the char structure.

Fig. 6 illustrates how A_D/A_{ALL} changes with H/C and O/C atomic

ratios of char. It can be seen in Fig. 6 that the ratio A_D/A_{ALL} generally increases as the elemental ratios fall. This means that when the amount of carbon in a compound increases and the concentrations of hydrogen and oxygen decreases, much more big aromatic rings are observed at the same time. In other words, the pyrolysis process converts the disordered carbon structure of the char into a more ordered one by removing the hydrogen and oxygen content. The R^2 values for the correlations between A_D/A_{ALL} and H/C and between A_D/A_{ALL} and O/C are roughly 0.75 and 0.69, respectively, which also shows that changes in the order degree of the large aromatic ring systems are more related to the dehydrogenation process during the pyrolysis process.

The G_L band is connected to the O-containing functional groups in char, as was discussed in Section 3.2, and it primarily just reflects the carbonyl C=O group. Because of this, the relative intensity of the G_L band can be used to show the relative content of the carbonyl C=O compounds in char [30]. Fig. 7 depicts how H/C and O/C affect the ratios between the area of the G_L band and the total area of all bands (A_{GL}/A_{ALL}). It is clear to see that the ratio of A_{GL}/A_{ALL} goes down in a continuous fashion as the two elemental ratios go down, and the R^2 values for the linear fitting are approximately 0.74 and 0.77, accordingly. It can be inferred that, during the pyrolysis process,

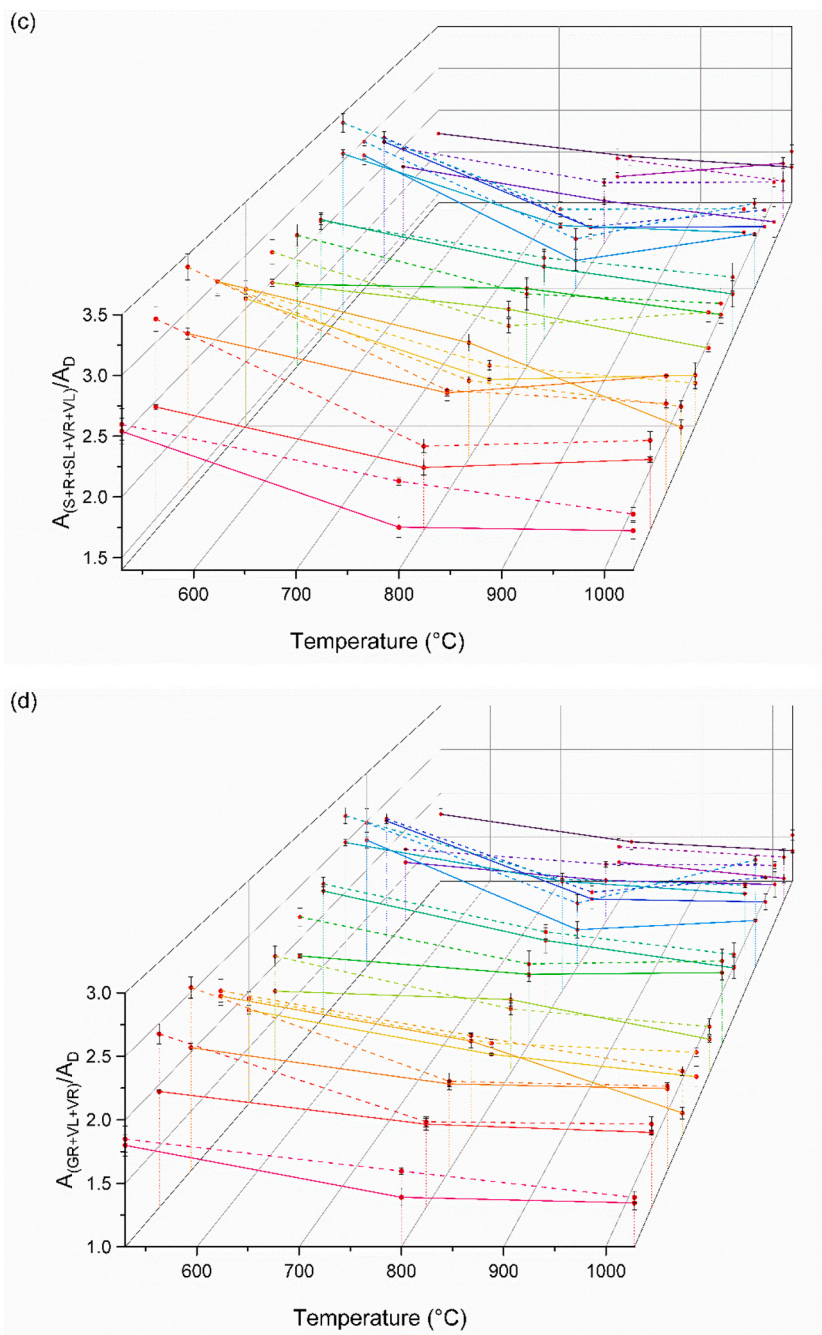


Fig. 5. (continued).

concentrations of the carbonyl C=O group structures in the char decrease in a linear way as the amount of carbon in the char goes up and the amounts of hydrogen and oxygen go down. The relatively stronger linear relationship between A_{GL}/A_{ALL} and O/C compared to the correlation between A_{GL}/A_{ALL} and H/C also implies that the change in the oxygen content of the char can better reflect the evolution of A_{GL}/A_{ALL} and the carbonyl C=O group may be an essential element of the O-containing groups in the char.

Fig. 8 exhibits the variation that takes place in the ratio of the area of the S, R, S_L , V_R , and V_L bands to the area of the D band as a function of the H/C and O/C values. It should be unsurprising to point out that the ratio $A_{(S+R+SL+VR+VL)}/A_D$ drops as the elemental ratios fall to the lower values. According to Table 1, C—C on alkanes and cyclic alkanes, the $C_{aromatic-C_{alkyl}}$, aromatic (aliphatic) ethers, aryl-alkyl ether, methylene, and methyl groups, etc., can be primarily responsible for the area of the

S, R, S_L , V_R , and V_L bands [29,41]. Therefore, the relative strength of the area of the S, R, S_L , V_R , and V_L bands can be used to represent the structures in the char that contain oxygen atoms and those that have partial sp^3 properties. The relationship between the significantly less well-organized structures and the large aromatic rings in char is revealed by calculating the ratio $A_{(S+R+SL+VR+VL)}/A_D$. There will be fewer aliphatic, hydro-aromatic, or O-containing functional groups in char because of the increasing condensation of the aromatic rings, resulting in a relatively lower degree of the ratio $A_{(S+R+SL+VR+VL)}/A_D$ [41,44]. This trend also can be reflected by the loss of hydrogen and oxygen as a char with a higher degree of order is thought to have lower hydrogen and oxygen contents [2,37]. The values of R^2 for the two correlations (0.72 and 0.69) are relatively low, which can be explained by the complexity of the structures represented by these bands and cannot be easily reflected by the C, H, and O elemental ratios.

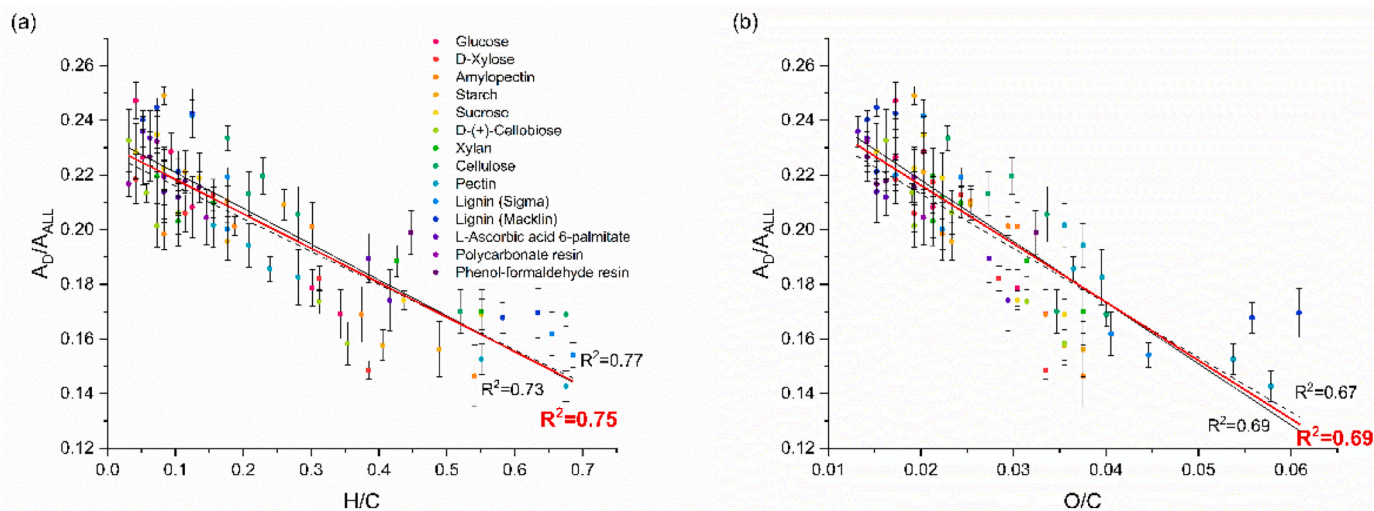


Fig. 6. Raman band area ratio A_D/A_{ALL} as a function of ratios of organic composition (a)H/C and (b)O/C. The solid black line represents the linear fitting of char from a fast heating rate, the dash black line represents the linear fitting of char from a slow heating rate, and the red line represents the linear fitting of all char samples. (For interpretation of the references to colour in this figure legend, the reader is referred to the web version of this article.)

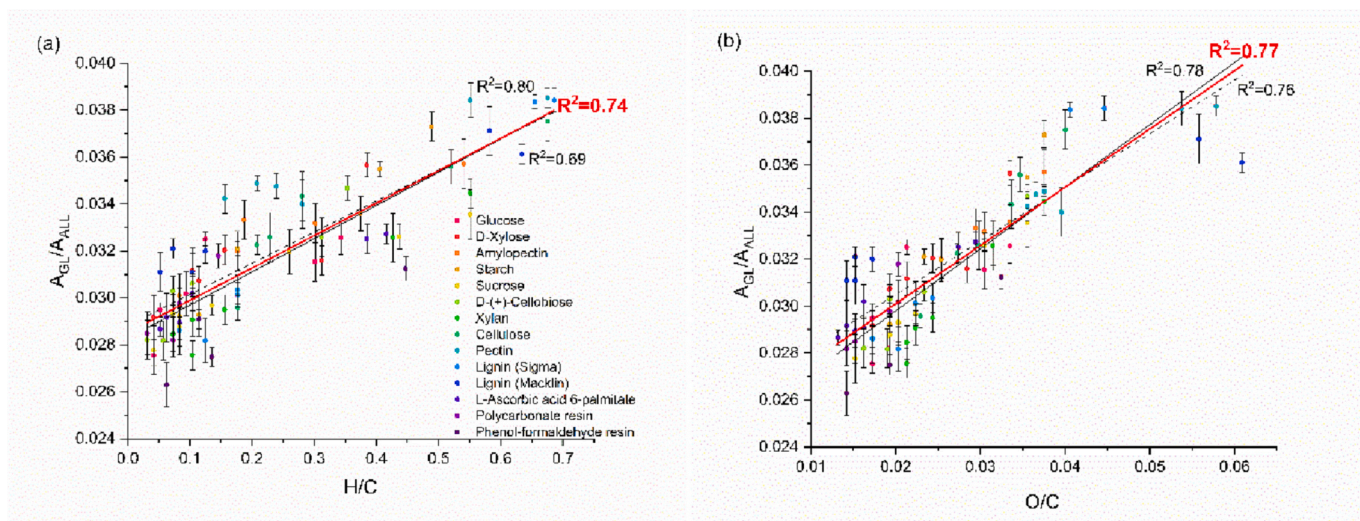


Fig. 7. Raman band area ratio A_{GL}/A_{ALL} as a function of ratios of organic composition (a)H/C and (b)O/C. The solid black line represents the linear fitting of char from a fast heating rate, the dash black line represents the linear fitting of char from a slow heating rate, and the red line represents the linear fitting of all char samples. (For interpretation of the references to colour in this figure legend, the reader is referred to the web version of this article.)

Fig. 9 depicts the connection between $A_{(GR+VL+VR)}/A_D$ and the H/C and O/C ratios of the char. The ratio $A_{(GR+VL+VR)}/A_D$ is used for the representation of the ratios of the small aromatic rings to the large ones in the char. As shown in Fig. 9, the ratio $A_{(GR+VL+VR)}/A_D$ generally decreases as the values of both two elemental ratios decrease, which indicates that there are fewer small aromatic rings while larger ones in char that have a higher content of carbon but a lower content of hydrogen and oxygen. In other words, the process of carbonization would result in the combination of the smaller aromatic rings and subsequently lead to the formation of larger ones [59], which is accompanied by the dehydrogenation and deoxygenation process that can be indicated by the decrease in the relative amounts of the hydrogen and oxygen contents. The R^2 values for the correlations between $A_{(GR+VL+VR)}/A_D$ and the elemental ratios are 0.75 and 0.77, respectively. These values are generally the highest among the four Raman parameters shown above, indicating that the condensation of the smaller aromatic systems into larger ones is the primary reaction occurring throughout the pyrolysis. Thus, higher carbon content and lower

hydrogen and oxygen content may be used to represent the carbon structures with fewer small aromatic ring systems and more large ones.

The correlations between the Raman parameters and the elemental ratios of char from respectively slow and fast heating, are also shown in Fig. 6-9. Similar to Fig. 4, these correlations also show no difference within the margin of error for char from the two different heating rates.

3.4. The relationships between Raman spectral parameters and char reactivity

The char oxidation reactivity was investigated with the combustion characteristic temperatures defined previously in Section 2.5, and the four characteristic temperatures: T_i , T_b , T_{50} , and T_{max} for all char samples were summarized in Table S2. Since char with high characteristic temperatures well represent char with low reactivity, the correlations between the characteristic temperatures and the Raman spectral parameters can be used for the investigation of the relationships between char structure and reactivity. Information about the correlations are

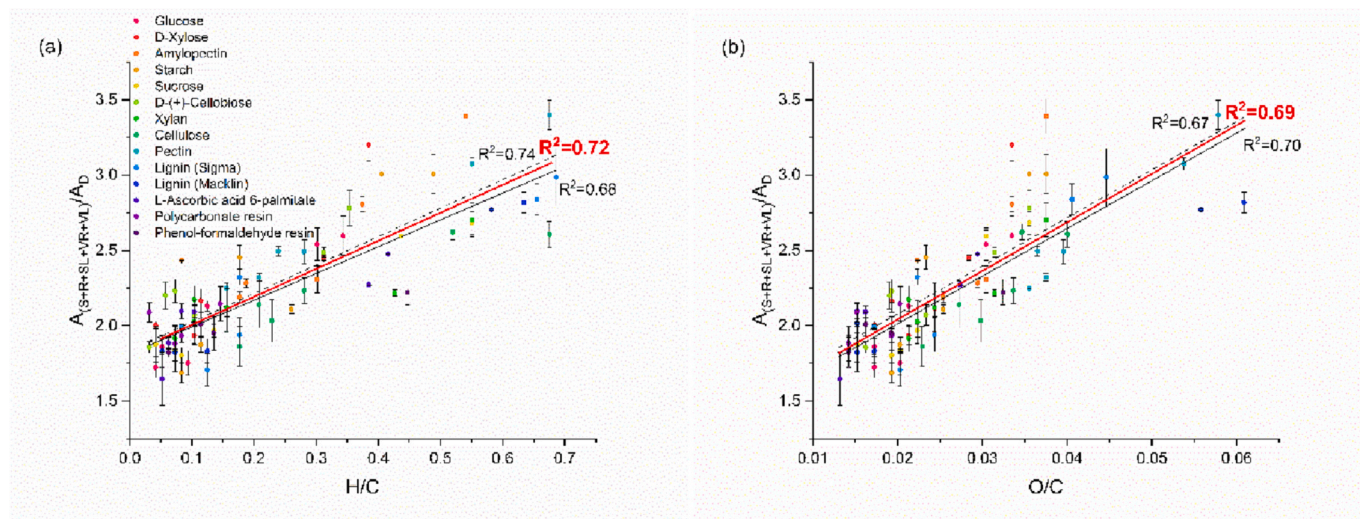


Fig. 8. Raman band area ratio $A_{(S+R+SL+VR+VL)}/A_D$ as a function of ratios of organic composition (a) H/C and (b) O/C. The solid black line represents the linear fitting of char from a fast heating rate, the dash black line represents the linear fitting of char from a slow heating rate, and the red line represents the linear fitting of all char samples. (For interpretation of the references to colour in this figure legend, the reader is referred to the web version of this article.)

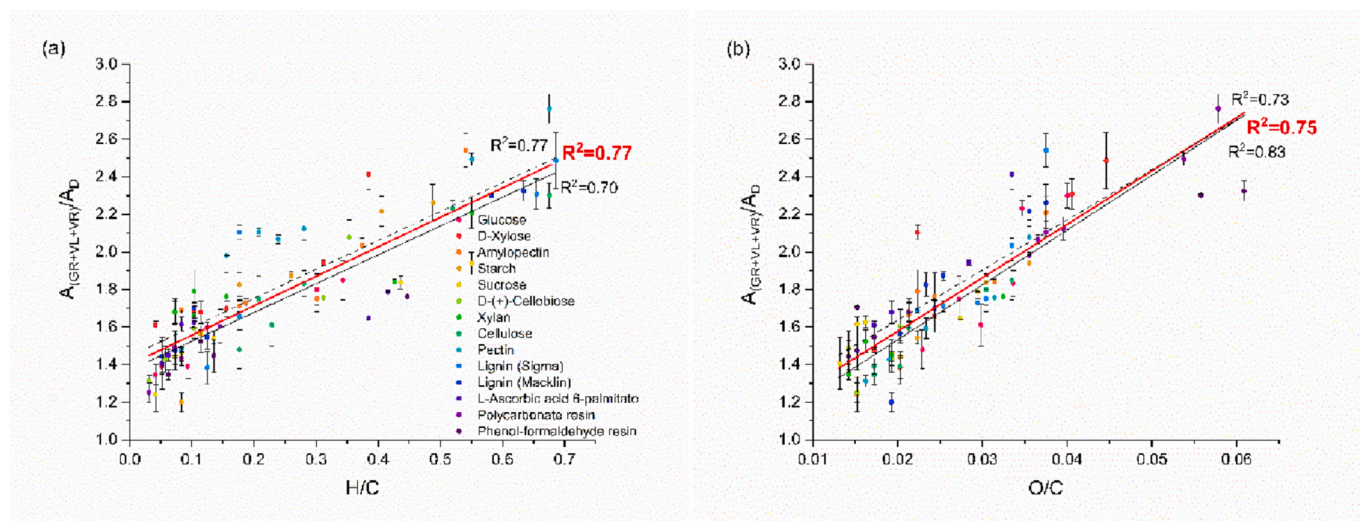


Fig. 9. Raman band area ratio $A_{(GR+VL+VR)}/A_D$ as a function of ratios of organic composition (a) H/C and (b) O/C. The solid black line represents the linear fitting of char from a fast heating rate, the dash black line represents the linear fitting of char from a slow heating rate, and the red line represents the linear fitting of all char samples. (For interpretation of the references to colour in this figure legend, the reader is referred to the web version of this article.)

provided in the Supplementary materials (Fig. S2-S5 and Table S3).

Fig. S2 shows the relationships between the four characteristic temperatures of the char and A_D/A_{ALL} . It is clear that the T_i , T_b , T_{50} , and T_{max} values all go up when the ratio A_D/A_{ALL} rises. As discussed in Section 3.2, the Raman spectral ratio A_D/A_{ALL} can indicate the Raman contribution from the large aromatic ring systems. It can be inferred that the increased contents of the large fused aromatic system in the char would make the char structure more ordered, thus leading to the phenomenon that the char becomes harder to ignite and results in relatively higher characteristic temperatures, which shows that the char with a higher degree of order can lead to the lower reactivity. As can be seen in Fig. 10, the R^2 values for the correlation between the combustion characteristic temperatures T_i , T_b , T_{50} , and T_{max} and the Raman parameter A_D/A_{ALL} are approximately 0.55, 0.62, 0.63, and 0.55, respectively. It means that the correlations between the char combustion reactivity and A_D/A_{ALL} are modest, indicating that the condensation degree of the aromatic systems in char has some impact on its reactivity.

Fig. S3 illustrates the combustion characteristic temperatures as a

function of A_{GL}/A_{ALL} . T_i , T_b , T_{50} , and T_{max} values all experience a downward trend when the A_{GL}/A_{ALL} value is increased. The result can be explained by the fact that the carbonyl structure is quite active, which makes the chars easier to react during the combustion process [60]. In addition, it suggests that the reactivity of the char is influenced by the quantity of the C=O functional groups, which are contained inside the massive aromatic rings that make up the char. As there is a relatively strong correlation between the A_{GL}/A_{ALL} and the atomic ratios, as discussed in Section 3.3, there are also correlations between the characteristic temperatures and A_{GL}/A_{ALL} . R^2 is approximately 0.47, 0.69, 0.62, and 0.53 for the correlations with T_i , T_b , T_{50} , and T_{max} , respectively, which indicates that the carbonyl structure in the char is one of the factors that have an influence on char reactivity.

The connections between the temperatures that are indicative of the burning of char and $A_{(S+R+SL+VR+VL)}/A_D$ are displayed in Fig. S4. T_i , T_b , T_{50} , and T_{max} all decrease as $A_{(S+R+SL+VR+VL)}/A_D$ increases. It has been discussed before that the ratio $A_{(S+R+SL+VR+VL)}/A_D$ represents the structures with partial sp^3 characteristics and the structures containing

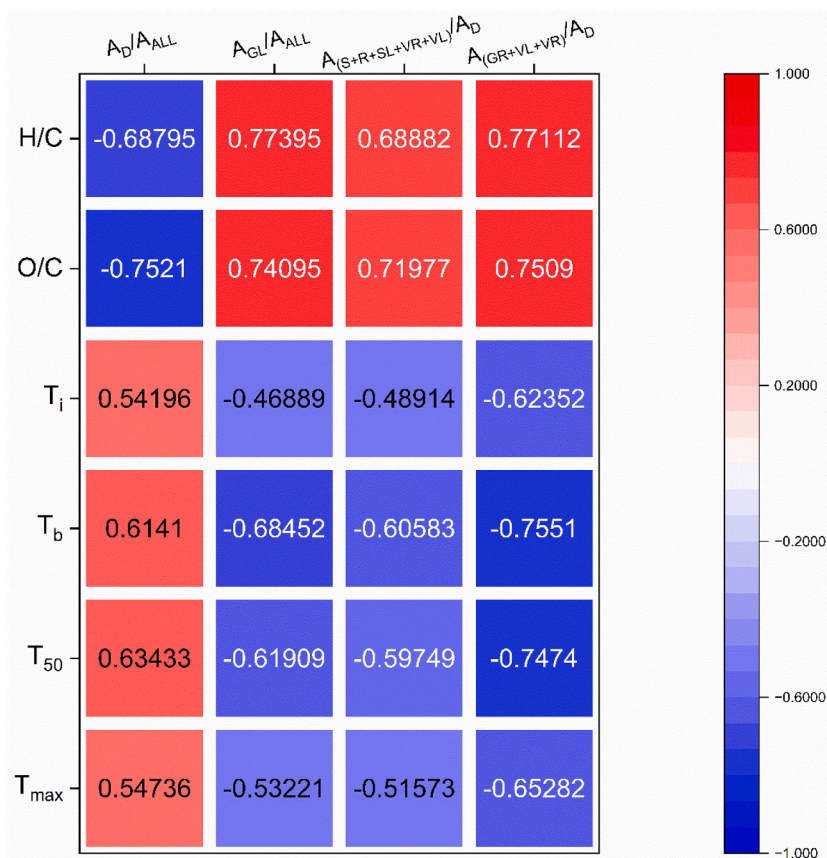


Fig. 10. Correlation coefficient R^2 of Raman spectral parameters on ratios of organic composition and combustion characteristic temperature. (red represents positive correlation, blue represents negative correlation). (For interpretation of the references to colour in this figure legend, the reader is referred to the web version of this article.)

oxygen, etc. These structures generally represent the active sites in the char conversion [46], which suggests that a char with a relatively higher content of such structures should burn easily and have lower combustion characteristic temperatures. The R^2 values for the correlation between T_i , T_b , T_{50} , and T_{max} and $A_{(S+R+SL+VR+VL)}/A_D$ are approximately 0.49, 0.61, 0.60, and 0.51, suggesting that there are also certain relationships between the char reactivity and $A_{(S+R+SL+VR+VL)}/A_D$.

Fig. S5 exhibits the relationships between T_i , T_b , T_{50} , and T_{max} and $A_{(GR+VL+VR)}/A_D$. The R^2 values are roughly 0.63, 0.76, 0.75, and 0.65, which are relatively larger when compared to other correlations above (as shown in Fig. S2-S4). It implies that the ratio $A_{(GR+VL+VR)}/A_D$ has a rather stronger relationship with the characteristic temperatures associated with the char combustion process. $A_{(GR+VL+VR)}/A_D$ can primarily represent the relative number of the smaller aromatic ring systems to larger ones in the char which is depicted in the Raman spectral as the valley that exists between D band and G band. The result infers that the concentration of the small aromatic rings in char is an important factor that affects the char combustion behavior. According to Asadullah et al. [12], large aromatic rings are relatively unreactive to the combustion reaction, and a higher degree of condensation will therefore lead to the char being converted at a relatively higher temperature. Thus, with a better correlation with the combustion characteristic temperature, $A_{(GR+VL+VR)}/A_D$ appears to be a crucial factor that affects the char combustion reactivity.

A higher A_D/A_{ALL} ratio and lower ratios of A_{GL}/A_{ALL} , $A_{(S+R+SL+VR+VL)}/A_D$, and $A_{(GR+VL+VR)}/A_D$ are linked to a higher order degree of carbon structures in char [30,41], which can also be verified by the high correlations between the Raman spectral parameters and the ratios H/C and O/C of the char, as shown in Fig. 10, that the lower H/C and O/C ratios are closely related to a higher order degree of char

structure. Fig. 10 shows the correlation coefficients obtained from the correlations of the Raman spectral parameters with the elemental ratios and the combustion characteristic temperatures, respectively. It's clear in Fig. 10 that the correlations between the characteristic temperatures and A_D/A_{ALL} is positive, while the correlations with the other three Raman spectral parameters are negative. The result infers that the higher order degree of char structure may lead to a higher combustion temperature, which means such chars are becoming harder to react throughout the combustion process. R^2 of the correlation with T_b appears to be the highest among the correlation values for all the four characteristic temperatures. In some ways, the temperature T_b can reflect the late stage of the reaction. This means that the carbon structure of the char, as described by the Raman spectroscopy, best matched the end-stage of the combustion characteristic of char. In addition, the correlation between T_b and $A_{(GR+VL+VR)}/A_D$ is shown as the best among the four correlations with T_b . It implies that the $A_{(GR+VL+VR)}/A_D$ ratio may be the best Raman spectral parameter to estimate the char combustion reactivity. Furthermore, the Raman spectroscopy test makes the acquiring of the $A_{(GR+VL+VR)}/A_D$ ratio easy and straightforward, which is beneficial for real-world applications of this technology.

The correlation is universal among all char samples investigated in the present study, which suggests that such an effect of carbon structure on char combustion behavior may exist in all the organic model compounds. It shows promise for further study of the impact of char structural properties on char combustion reactivity for real biomass, and it can also be inferred that such relationships can exist among various different carbonaceous solid fuels. Accordingly, further research is needed to investigate the chars from the practical application of real biomass for a better understanding of the effect of the carbon structure of char on char reactivity.

4. Conclusion

14 types of organic model compounds varying in their carbon contents were pyrolyzed under different conditions to obtain 84 char samples. TGA, Raman spectroscopy and elemental analysis were employed to explore the relationships between combustion reactivity and composition structures of chars. The conclusions are drawn as follows:

- (1) Higher temperatures and heating rates reduce char yield, with the latter having a greater effect. The Raman spectroscopy reveals that the condensation from the small aromatic ring systems to large ones and the graphitization of the char structure becomes more pronounced as the pyrolysis temperature increases and the heating rate decreases, probably because of the extended residence time.
- (2) The carbon structures characterized by the Raman spectral parameters A_D/A_{ALL} , A_{GL}/A_{ALL} , $A_{(S+R+SL+VR+VL)}/A_D$, and $A_{(GR+VL+VR)}/A_D$ can be well reflected by the content of C, H, and O atoms in the char. The increase in the C content and decrease in the H and O content can represent the condensation of the aromatic ring systems and the consumption of the O-containing functional groups and sp^3 structures in the char that has a higher degree of order.
- (3) Clear linear correlations have been discovered between the char combustion characteristic temperatures (T_i , T_b , T_{50} , and T_{max}) and the Raman spectral parameters. The increasing graphitization degree, consumption of carbonyl structures, and condensation of small ring systems revealed by the Raman spectral parameters are related closely to the increase of the characteristic temperatures, which in turn are related to low char reactivity. $A_{(GR+VL+VR)}/A_D$ is the best among all correlated Raman parameters. The high correlations reveal that Raman spectroscopy is a useful technique for the investigation of char structure and can be used to estimate char combustion reactivity.

CRedit authorship contribution statement

Zhengyan Bao: Investigation, Methodology, Writing – original draft. **Zhimin Lu:** Conceptualization, Funding acquisition, Supervision, Writing – review & editing. **Jinzheng Chen:** Methodology, Writing – review & editing. **Jianfeng Cai:** Writing – review & editing. **Shengyuan Guo:** Writing – review & editing. **Shunchun Yao:** Funding acquisition, Resources, Supervision.

Declaration of Competing Interest

The authors declare that they have no known competing financial interests or personal relationships that could have appeared to influence the work reported in this paper.

Data availability

Data will be made available on request.

Acknowledgements

This work was supported by the National Natural Science Foundation of China (52276190), the Natural Science Foundation of Guangdong Province (2022A1515010741) and the Fundamental Research Funds for the Central Universities (2022ZFJH004).

Appendix A. Supplementary data

Supplementary data to this article can be found online at <https://doi.org/10.1016/j.fuproc.2023.107852>.

References

- [1] X. Chen, H. Wu, Volatile-char interactions: Roles of in situ volatiles with distinctly-different chemistry in determining char structure and reactivity, *Proc. Combust. Inst.* 37 (2019) 2749–2755, <https://doi.org/10.1016/j.proci.2018.05.019>.
- [2] M. Morin, S. Pécate, M. Hémati, Y. Kara, Pyrolysis of biomass in a batch fluidized bed reactor: effect of the pyrolysis conditions and the nature of the biomass on the physicochemical properties and the reactivity of char, *J. Anal. Appl. Pyrolysis* 122 (2016) 511–523, <https://doi.org/10.1016/j.jaap.2016.10.002>.
- [3] G.R. Surup, M. Foppe, D. Schubert, R. Deike, M. Heidelmann, M.T. Timko, et al., The effect of feedstock origin and temperature on the structure and reactivity of char from pyrolysis at 1300–2800 °C, *Fuel* 235 (2019) 306–316, <https://doi.org/10.1016/j.fuel.2018.07.093>.
- [4] J. Yu, Q. Guo, L. Ding, Y. Gong, G. Yu, Studying effects of solid structure evolution on gasification reactivity of coal chars by in-situ Raman spectroscopy, *Fuel* 270 (2020), 117603, <https://doi.org/10.1016/j.fuel.2020.117603>.
- [5] A. Phounglamcheik, L. Wang, H. Romar, N. Kienzl, M. Broström, K. Ramser, et al., Effects of Pyrolysis Conditions and Feedstocks on the Properties and Gasification Reactivity of Charcoal from Woodchips, *Energy Fuel* 34 (2020) 8353–8365, <https://doi.org/10.1021/acs.energyfuels.0c00592>.
- [6] C. Guizani, M. Jeguirim, R. Gadiou, F.J. Escudero Sanz, S. Salvador, Biomass char gasification by H₂O, CO₂ and their mixture: Evolution of chemical, textural and structural properties of the chars, *Energy* 112 (2016) 133–145, <https://doi.org/10.1016/j.energy.2016.06.065>.
- [7] Z. Bouraoui, C. Dupont, M. Jeguirim, L. Limousy, R. Gadiou, CO₂ gasification of woody biomass chars: the influence of K and Si on char reactivity, *C. R. Chim. Iv* 9 (2016) 457–465, <https://doi.org/10.1016/j.crci.2015.08.012>.
- [8] C. Hognon, C. Dupont, M. Grateau, F. Delrue, Comparison of steam gasification reactivity of algal and lignocellulosic biomass: Influence of inorganic elements, *Bioresour. Technol.* 164 (2014) 347–353, <https://doi.org/10.1016/j.biortech.2014.04.111>.
- [9] C. Dupont, S. Jacob, K.O. Marrakchy, C. Hognon, M. Grateau, F. Labalette, et al., How inorganic elements of biomass influence char steam gasification kinetics, *Energy* 109 (2016) 430–435, <https://doi.org/10.1016/j.energy.2016.04.094>.
- [10] S. Li, H. Song, J. Hu, H. Yang, J. Zou, Y. Zhu, et al., CO₂ gasification of straw biomass and its correlation with the feedstock characteristics, *Fuel* 297 (2021), 120780, <https://doi.org/10.1016/j.fuel.2021.120780>.
- [11] X. Li, J. He, M. Liu, J. Bai, Z. Bai, W. Li, Interaction between coal and Biomass during Co-Gasification: a Perspective based on the separation of blended char, *Processes* 10 (2022) 1–14, <https://doi.org/10.3390/pr10020286>.
- [12] M. Asadullah, S. Zhang, Z. Min, P. Yimsiri, C.Z. Li, Effects of biomass char structure on its gasification reactivity, *Bioresour. Technol.* 101 (2010) 7935–7943, <https://doi.org/10.1016/j.biortech.2010.05.048>.
- [13] H. Wu, K. Yip, F. Tian, Z. Xie, C.-Z. Li, Evolution of Char Structure during the Steam Gasification of Biochars Produced from the Pyrolysis of various Mallee Biomass Components, *Ind. Eng. Chem. Res.* 48 (2009) 10431–10438, <https://doi.org/10.1021/ie901025d>.
- [14] H.L. Tay, S. Kajitani, S. Zhang, C.Z. Li, Effects of gasifying agent on the evolution of char structure during the gasification of Victorian brown coal, *Fuel* 103 (2013) 22–28, <https://doi.org/10.1016/j.fuel.2011.02.044>.
- [15] H. Tian, Y. Wei, S. Cheng, Z. Huang, M. Qing, Y. Chen, et al., Optimizing the gasification reactivity of biochar: the composition, structure and kinetics of biochar derived from biomass lignocellulosic components and their interactions during gasification process, *Fuel* 324 (2022), 124709, <https://doi.org/10.1016/j.fuel.2022.124709>.
- [16] K. Lotz, C.M. Berger, M. Muhler, Catalytic effect of iron phases on the oxidation of cellulose-derived synthetic char, *Energy Procedia* 158 (2019) 694–699, <https://doi.org/10.1016/j.egypro.2019.01.188>.
- [17] H. Düdler, A. Wütscher, R. Stoll, M. Muhler, Synthesis and characterization of lignite-like fuels obtained by hydrothermal carbonization of cellulose, *Fuel* 171 (2016) 54–58, <https://doi.org/10.1016/j.fuel.2015.12.031>.
- [18] H. Düdler, K. Lotz, A. Wütscher, M. Muhler, The influence of iron oxide on the oxidation kinetics of synthetic char derived from thermogravimetric analysis and fixed-bed experiments under isothermal and temperature-programmed conditions, *Fuel* 201 (2017) 99–104, <https://doi.org/10.1016/j.fuel.2016.09.076>.
- [19] T. Lang, R.H. Hurt, Char combustion reactivities for a suite of diverse solid fuels and char-forming organic model compounds, *Proc. Combust. Inst.* 29 (2002) 423–431, [https://doi.org/10.1016/S1540-7489\(02\)80056-6](https://doi.org/10.1016/S1540-7489(02)80056-6).
- [20] S. Zhang, S. Yu, Q. Li, B.A. Mohamed, Y. Zhang, H. Zhou, Insight into the relationship between CO₂ gasification characteristics and char structure of biomass, *Biomass Bioenergy* 163 (2022), 106537, <https://doi.org/10.1016/j.biombioe.2022.106537>.
- [21] T. Kato, Y. Yamada, Y. Nishikawa, H. Ishikawa, S. Sato, Carbonization mechanisms of polyimide: Methodology to analyze carbon materials with nitrogen, oxygen, pentagons, and heptagons, *Carbon N Y* 178 (2021) 58–80, <https://doi.org/10.1016/j.carbon.2021.02.090>.
- [22] Y. Zhang, Q. Shang, D. Feng, H. Sun, F. Wang, Z. Hu, et al., Interaction mechanism of in-situ catalytic coal H₂O-gasification over biochar catalysts for H₂O-H₂-tar reforming and active sites conversion, *Fuel Process. Technol.* 233 (2022), 107307, <https://doi.org/10.1016/j.fuproc.2022.107307>.
- [23] J. Xu, Q. He, Z. Xiong, Y. Yu, S. Zhang, X. Hu, et al., Raman Spectroscopy as a Versatile Tool for Investigating Thermochemical Processing of coal, Biomass, and Wastes: recent advances and Future Perspectives, *Energy Fuel* 35 (2021) 2870–2913, <https://doi.org/10.1021/acs.energyfuels.0c03298>.
- [24] J. Xu, J. Liu, P. Ling, X. Zhang, K. Xu, L. He, et al., Raman spectroscopy of biochar from the pyrolysis of three typical Chinese biomasses: a novel method for rapidly

- evaluating the biochar property, *Energy* 202 (2020), 117644, <https://doi.org/10.1016/j.energy.2020.117644>.
- [25] C. Guizani, M. Jeguirim, S. Valin, L. Limousy, S. Salvador, Biomass chars: the effects of pyrolysis conditions on their morphology, structure, chemical properties and reactivity, *Energies* 10 (2017) 796, <https://doi.org/10.3390/en10060796>.
- [26] D. Zhong, Z. Chang, K. Zeng, J. Li, Y. Qiu, Q. Lu, et al., Solar pyrolysis of biomass - part II: the physicochemical structure evolution of char, *Fuel* 333 (2023), 126474, <https://doi.org/10.1016/j.fuel.2022.126474>.
- [27] Y. Li, D. Feng, S. Sun, Y. Zhao, Q. Shang, K. Chen, et al., Biomass-coal reburning: Competitive mechanism of gas-solid product activation coal char, *Energy* 261 (2022), 125225, <https://doi.org/10.1016/j.energy.2022.125225>.
- [28] J. Jian, Z. Lu, S. Yao, Y. Li, Z. Liu, B. Lang, et al., Effects of thermal conditions on char yield and char reactivity of woody biomass in stepwise pyrolysis, *J. Anal. Appl. Pyrolysis* 138 (2019) 211–217, <https://doi.org/10.1016/j.jaap.2018.12.026>.
- [29] X. Li, J. Hayashi, ichiro, Li CZ., FT-Raman spectroscopic study of the evolution of char structure during the pyrolysis of a Victorian brown coal, *Fuel* 85 (2006) 1700–1707, <https://doi.org/10.1016/j.fuel.2006.03.008>.
- [30] J. Xu, H. Tang, S. Su, J. Liu, K. Xu, K. Qian, et al., A study of the relationships between coal structures and combustion characteristics: the insights from micro-Raman spectroscopy based on 32 kinds of Chinese coals, *Appl. Energy* 212 (2018) 46–56, <https://doi.org/10.1016/j.apenergy.2017.11.094>.
- [31] X. Zhu, C. Sheng, Influences of carbon structure on the reactivities of lignite char reacting with CO₂ and NO, *Fuel Process. Technol.* 91 (2010) 837–842, <https://doi.org/10.1016/j.fuproc.2009.10.015>.
- [32] J. Xu, S. Su, Z. Sun, M. Qing, Z. Xiong, Y. Wang, et al., Effects of steam and CO₂ on the characteristics of chars during devolatilization in oxy-steam combustion process, *Appl. Energy* 182 (2016) 20–28, <https://doi.org/10.1016/j.apenergy.2016.08.121>.
- [33] C. Zou, J. Zhao, X. Li, R. Shi, Effects of catalysts on combustion reactivity of anthracite and coal char with low combustibility at low/high heating rate, *J. Therm. Anal. Calorim.* 126 (2016) 1469–1480, <https://doi.org/10.1007/s10973-016-5806-y>.
- [34] J. Cheng, F. Zhou, X. Xuan, J. Liu, J. Zhou, K. Cen, Cascade chain catalysis of coal combustion by Na–Fe–Ca composite promoters from industrial wastes, *Fuel* 181 (2016) 820–826, <https://doi.org/10.1016/j.fuel.2016.05.064>.
- [35] X. Zhang, Y. Liu, C. Wang, D. Che, Experimental study on interaction and kinetic characteristics during combustion of blended coals, *J. Therm. Anal. Calorim.* 107 (2012) 935–942, <https://doi.org/10.1007/s10973-011-1657-8>.
- [36] B. Zhao, D. O'Connor, J. Zhang, T. Peng, Z. Shen, D.C.W. Tsang, et al., Effect of pyrolysis temperature, heating rate, and residence time on rapeseed stem derived biochar, *J. Clean. Prod.* 174 (2018) 977–987, <https://doi.org/10.1016/j.jclepro.2017.11.013>.
- [37] C. Guizani, K. Haddad, L. Limousy, M. Jeguirim, New insights on the structural evolution of biomass char upon pyrolysis as revealed by the Raman spectroscopy and elemental analysis, *Carbon N Y* 119 (2017) 519–521, <https://doi.org/10.1016/j.carbon.2017.04.078>.
- [38] S. Xin, H. Yang, Y. Chen, M. Yang, L. Chen, X. Wang, et al., Chemical structure evolution of char during the pyrolysis of cellulose, *J. Anal. Appl. Pyrolysis* 116 (2015) 263–271, <https://doi.org/10.1016/j.jaap.2015.09.002>.
- [39] T. Li, L. Zhang, L. Dong, P. Qiu, S. Wang, S. Jiang, et al., Changes in char structure during the low-temperature pyrolysis in N₂ and subsequent gasification in air of Loy Yang brown coal char, *Fuel* 212 (2018) 187–192, <https://doi.org/10.1016/j.fuel.2017.10.026>.
- [40] X. Li, J. Hayashi, ichiro, Li CZ., Volatilisation and catalytic effects of alkali and alkaline earth metallic species during the pyrolysis and gasification of Victorian brown coal. Part VII. Raman spectroscopic study on the changes in char structure during the catalytic gasification in air, *Fuel* 85 (2006) 1509–1517, <https://doi.org/10.1016/j.fuel.2006.01.011>.
- [41] D.M. Keown, X. Li, J. Hayashi, C.-Z. Li, Evolution of biomass char structure during oxidation in O₂ as revealed with FT-Raman spectroscopy, *Fuel Process. Technol.* 89 (2008) 1429–1435, <https://doi.org/10.1016/j.fuproc.2008.07.002>.
- [42] R. Morga, Micro-Raman spectroscopy of carbonized semifusinite and fusinite, *Int. J. Coal Geol.* 87 (2011) 253–267, <https://doi.org/10.1016/j.coal.2011.06.016>.
- [43] M.W. Smith, I. Dallmeyer, T.J. Johnson, C.S. Brauer, J.-S. McEwen, J.F. Espinal, et al., Structural analysis of char by Raman spectroscopy: improving band assignments through computational calculations from first principles, *Carbon N Y* 100 (2016) 678–692, <https://doi.org/10.1016/j.carbon.2016.01.031>.
- [44] N. Li, Y. Wang, S. Cui, D. Sun, Investigations on NO reduction with biomass char: char structural changes during the heat treatment in N₂ and subsequent NO/O₂ gasification, *Fuel* 287 (2021), <https://doi.org/10.1016/j.fuel.2020.119564>, 119564.
- [45] Q. Xu, Z. Liu, H. Jiang, Q. Zhang, C. Zan, D. Ma, et al., Chemical-structural properties of the coke produced by low temperature oxidation reactions during crude oil in-situ combustion, *Fuel* 207 (2017) 179–188, <https://doi.org/10.1016/j.fuel.2017.06.026>.
- [46] Y. Xie, H. Yang, K. Zeng, Y. Zhu, J. Hu, Q. Mao, et al., Study on CO₂ gasification of biochar in molten salts: Reactivity and structure evolution, *Fuel* (2019) 254, <https://doi.org/10.1016/j.fuel.2019.06.022>.
- [47] S. Wang, L. Wu, X. Hu, L. Zhang, T. Li, C.-Z. Li, Effects of the Particle size and Gasification Atmosphere on the changes in the Char Structure during the Gasification of Mallee Biomass, *Energy Fuel* 32 (2018) 7678–7684, <https://doi.org/10.1021/acs.energyfuels.8b01309>.
- [48] X. Hu, K. Nango, L. Bao, T. Li, M.D. Mahmudul Hasan, C.Z. Li, High yields of solid carbonaceous materials from biomass, *Green Chem.* 21 (2019) 1128–1140, <https://doi.org/10.1039/c8gc03153c>.
- [49] Y. Liu, M. Paskevicius, M.V. Sofianos, G. Parkinson, S. Wang, C.Z. Li, A SAXS study of the pore structure evolution in biochar during gasification in H₂O, CO₂ and H₂O/CO₂, *Fuel* 292 (2021), 120384, <https://doi.org/10.1016/j.fuel.2021.120384>.
- [50] Y. Chen, S.S.A. Syed-Hassan, Q. Li, Z. Deng, X. Hu, J. Xu, et al., Effects of temperature and aspect ratio on heterogeneity of the biochar from pyrolysis of biomass pellet, *Fuel Process. Technol.* 235 (2022), 107366, <https://doi.org/10.1016/j.fuproc.2022.107366>.
- [51] B. Li, J. Tang, X. Xie, J. Wei, D. Xu, L. Shi, et al., Char structure evolution during molten salt pyrolysis of biomass: effect of temperature, *Fuel* 331 (2023), 125747, <https://doi.org/10.1016/j.fuel.2022.125747>.
- [52] D.M. Keown, X. Li, J. Hayashi, C.-Z. Li, Characterization of the Structural Features of Char from the Pyrolysis of Cane Trash using Fourier Transform–Raman Spectroscopy, *Energy Fuel* 21 (2007) 1816–1821, <https://doi.org/10.1021/ef070049r>.
- [53] S. Su, Y. Song, Y. Wang, T. Li, S. Hu, J. Xiang, et al., Effects of CO₂ and heating rate on the characteristics of chars prepared in CO₂ and N₂ atmospheres, *Fuel* 142 (2015) 243–249, <https://doi.org/10.1016/j.fuel.2014.11.025>.
- [54] M. Keiluweit, P.S. Nico, M. Johnson, M. Kleber, Dynamic molecular structure of plant biomass-derived black carbon (biochar), *Environ. Sci. Technol.* 44 (2010) 1247–1253, <https://doi.org/10.1021/es9031419>.
- [55] B.C.C. Fernandes, K.F. Mendes, A.F.D. Júnior, V.P. da S Caldeira, T.M. da S Teófilo, T.S. Silva, et al., Impact of pyrolysis temperature on the properties of eucalyptus wood-derived biochar, *Materials (Basel)* 13 (2020) 1–13, <https://doi.org/10.3390/ma13245841>.
- [56] C. Fushimi, K. Araki, Y. Yamaguchi, A. Tsutsumi, Effect of heating rate on steam gasification of biomass. 1. Reactivity of char, *Ind. Eng. Chem. Res.* 42 (2003) 3922–3928, <https://doi.org/10.1021/ie030056c>.
- [57] A.R.A. Usman, A. Abduljabbar, M. Vithanage, Y.S. Ok, M. Ahmad, M. Ahmad, et al., Biochar production from date palm waste: Charring temperature induced changes in composition and surface chemistry, *J. Anal. Appl. Pyrolysis* 115 (2015) 392–400, <https://doi.org/10.1016/j.jaap.2015.08.016>.
- [58] K. Yip, M. Xu, C.Z. Li, S.P. Jiang, H. Wu, Biochar as a fuel: 3. Mechanistic understanding on biochar thermal annealing at mild temperatures and its effect on biochar reactivity, *Energy Fuel* 25 (2011) 406–414, <https://doi.org/10.1021/ef101472f>.
- [59] T. Li, L. Zhang, L. Dong, S. Zhang, P. Qiu, S. Wang, et al., Effects of gasification temperature and atmosphere on char structural evolution and AAEM retention during the gasification of Loy Yang brown coal, *Fuel Process. Technol.* 159 (2017) 48–54, <https://doi.org/10.1016/j.fuproc.2017.01.022>.
- [60] L. Zhang, T. Li, S. Wang, L. Dong, C.Z. Li, Effects of alkali and alkaline earth metallic species and chemical structure on nascent char-O₂ reactivity, *Energy Fuel* 31 (2017) 13578–13584, <https://doi.org/10.1021/acs.energyfuels.7b03022>.